8610 *Macromolecules* **2010**, *43*, 8610–8618
DOI: 10.1021/ma1015566

Macromolecules
ARTICLE

# Polymorphic Crystallization and Phase Transition of Poly(butylene adipate) in Its Miscible Crystalline/Crystalline Blend with Poly(vinylidene fluoride)

**Jinjun Yang, Pengju Pan, Lei Hua, Bo Zhu, Tungalag Dong, and Yoshio Inoue***

*Department of Biomolecular Engineering, Tokyo Institute of Technology, 4259-B-55 Nagatsuta, Midori-ku, Yokohama 226-8501, Japan*

*Received July 11, 2010; Revised Manuscript Received September 1, 2010*

ABSTRACT: The effects of poly(vinylidene fluoride) (PVDF) component on the crystallization kinetics, crystalline structure, phase transition, and morphology of polymorphic poly(butylene adipate) (PBA) in their miscible PVDF/PBA binary blends have been investigated. The polymorphism of PBA can be regulated upon blending with PVDF. The incorporated PVDF faciliates the formation of PBA α-crystal, which is probably attributed to the thermodynamic and kinetic contributions. From the crystallization kinetics, it was found that a small amount of PVDF acts as a nucleating agent and can accelerate the crystallization of PBA, while a large amount of PVDF hinders the crystallization of PBA due to the confinement effect. In addition, the addition of PVDF greatly accelerates the $\beta$- to α-form phase transition of PBA upon annealing the PBA $\beta$-form at higher tmeperataure (48 °C). However, the large amount of PVDF decelerates the phase transition to a certain extent. The possible reasons for these phenomena were also proposed.

## Introduction

In order to improve the mechanical and physical properties of polymeric materials, which depend strongly on the morphology and crystalline structure, many works have been conducted on the polymer blending and copolymerization. Because of the simpleness and economy, the blending method has been widely employed in the property modification of polymers.[1,2] For example, the ternary blend, thermoplastic starch (TPS)/poly(lactic acid) (PLA)/poly(butylene adipate-*co*-terephthalate) (PBAT), exhibits a dramatic improvement in elongation at break with increasing the PBAT content.[1] After addition of PBAT, the foaming rate of PLA/PBAT blend is raised by nearly 50% than that of the pure PLA foams.[3] Upon blending with poly(ethylene succinate) (PES), the elongation at break of PLA is improved significantly in the PES/PLA binary blend pair.[4]

Poly(butylene adipate) (PBA) is a representative biodegradable linear aliphatic polyester that has potential biomedical applications.[5] PBA can crystallize into two kinds of crystalline phase, denoted as the α-form (the crystallization temperature $T_c \geq 32$ °C) and the $\beta$-form ($T_c \leq 28$ °C).[6−11] The PBA $\beta$-form can completely transform into the α-form upon heating or annealing at higher temperature.[5,9] Although the PBA α-form is thermodynamically stable, it shows the faster biodegradation. The PBA $\beta$-form is considered to be kinetically stable and shows the slower degradation rate than the α-form.[12]

Several studies have been reported to increase the crystallization rate and to control the polymorphism of PBA.[13,14] It has been reported that the inclusion complex (PBAIC) between PBA and α-cyclodextrin (α-CD) can effectively enhance the crystallization rate of PBA. With introduction of PBAIC, the full α-form crystal of PBA is preferentially formed.[13] With introduction of nucleating agents, such as talc, the nucleation of the PBA α-form crystal can be faciliated. Besides, the crystallization rate of the PBA α-form crystal is also increased.[14] Addition of another nucleating agent, multimethylbenzilidene sorbitol (TM6), is also favorable for the formation of the PBA α-form crystal.[15] Thus, the reduction of $T_c$ and enhancement of crystallization rate may be important for PBA to form the thermodynamically more stable α-crystal.

The epitaxial crystallization of PBA on the polyethylene (PE) or isotactic polypropylene (iPP) substrate results in the formation of the PBA $\beta$-crystal at any crystallization conditions due to the perfect lattice matching between the PBA $\beta$-crystal and the PE or iPP crystal.[16,17] This way can be a good choice to obtain the PBA $\beta$-crystal with lower biodegradation rate.[12] In addition, the so-called nuclei-memory effect[18] and complicated melting behavior[5] also influence significantly the polymorphism of PBA, which depends on the maxium melting temperature ($T_{max}$). It has been reported that the PBA $\beta$-crystal could be transformed into the α-crystal at a specific $T_{max}$ (e.g., 55 °C) at which the PBA α-crystal nuclei has not been erased completely.[18] Thus, the formed crysatal is found to be the α-crystal and $T_c$ does not affect the type of crystals. That is to say, only the α-crystal has the memory capacity in the molten state while the $\beta$-crystal does not. These methods have provided potential ways to control and regulate the crystalline modification of PBA.

Poly(vinylidene fluoride) (PVDF) is a semicrystalline and industrially important polymeric material which is used as protective layers and coating under severe physical conditions and chemical environments.[19] It is known that PVDF can exist in three crystal types, which have been denoted as the α-, $\beta$-, and $\gamma$-form.[20] PVDF melt-crystallized at below 160 °C is found to produce the spherulites of α-form.[21] The α-form can transform into the $\beta$-form by the orientation during the tensile process. The PVDF $\gamma$-form develops by melt-crystallization at above 160 °C or under the high pressure.[20,22]

In order to improve the mechanical property of PBA, the blend of PVDF/PBA has been prepared and investigated. The modulus and extensibility of PBA are increased after blending with PVDF.[23]

*To whom corresponding should be addressed: Tel +81-45-924-5794; Fax +81-45-924-5827; e-mail inoue.y.af@m.titech.ac.jp.

 Published on Web 09/21/2010 

Besides, the phase behavior, miscibility, and morphology of the PVDF/PBA blend system have been studied.[24−27] It was found that PVDF is miscible with PBA and PBA can be distributed in the interspherulitic or interlamellar/interfibrillar region of PVDF matrix depending on the content of the PVDF component ($C_{PVDF}$).

PVDF shows the melting point ($T_m$) of ~165 °C and the crystallization temperature ($T_c$) of ~140 °C.[25] The $T_m$ and $T_c$ of PBA are 50−60 and ~30 °C, respectively.[10,13] The $T_m$ and $T_c$ of PVDF are respectively much higher than those of PBA. Thus, their crystallization and melting behavior can be investigated separately in the PVDF/PBA blend. The PVDF/PBA blend system presents the different semicrystalline and/or amorphous state in the different temperature regions. Above the melting point of PVDF ($T_{m,PVDF}$), the blend is in a homogeneous and single-phase melt state. Decreasing the temperature to $T < T_{m,PVDF}$ leads to the crystallization of PVDF component, resulting in the transition from the fully amorphous and homogeneous state to the semicrystalline/amorphous two-phases state. Further lowering to the temperature below the melting point of PBA ($T < T_{m,PBA}$), the PBA component crystallizes as well, bringing the system from the semicrystalline/amorphous into the semicrystalline/semicrystalline three-phase state, that is, the crystalline PVDF, the crystalline PBA, and the amorphous PVDF/PBA mixed phase. Of course, the blend system can also be directly quenched from the homogeneous melt state of $T > T_{m,PVDF}$ to $T < T_{m,PBA}$ (that is, one-step crystallization) without undergoing the above-mentioned two-step crystallization. Therefore, the PVDF/PBA crystalline/crystalline blend, in which two components have remarkably different $T_m$s and $T_c$s, could be an interesting system. For this system, we can investigate the effect of the crystallization conditions of the high-$T_m$ component on the crystallization behavior and crystalline structure of the low-$T_m$ component.

It is well-known that the crystallization conditions affect significantly the crystalline structure, which is closely related to the mechanical and physical properties and biodegradability of biodegradable polymer.[5] In the poly(butylene succinate) (PBS)/poly(ethylene oxide) (PEO) blend pair, the crystallization behavior of the PEO component has been found to be highly affected by the crystallization temperature ($T_{c,PBS}$) and the content of PBS ($C_{PBS}$). Upon blending with PBS, PEO shows one, two, or three crystallization peaks, that is, the fractional crystallization, which significantly depends on $T_{c,PBS}$ and $C_{PBS}$.[28] The same issue will be easily proposed for the PVDF/PBA blend pair. How do the crystallization conditions of PVDF affect the crystallization behavior of PBA? Furthermore, it is more important that, in this article, the polymorphism and phase transition of PBA are first investigated in its semicrystalline/semicrystalline binary miscible blend. This blend pair is also anticipated to establish a model system to control and regulate the structure of polymorphic polymer in its semicrystalline/semicrystalline miscible blend.

In this work, the $C_{PVDF}$-dependent crystallization and melting behavior of the PBA component in the PVDF/PBA blend were investigated by differential scanning calorimetry (DSC). The effects of PVDF on the crystalline structure of PBA were elucidated by wide-angle X-ray diffraction (WAXD) and Fourier transform infrared (FTIR) spectroscopy. The phase transition of the PBA component by annealing in this blend system was also investigated by WAXD. Finally, the morphologies of the PVDF and PBA components in this blend system were oberved by polarized optical microscopy (POM).

## Experimental Section

**Materials.** PBA ($M_w$ = 12 000) was purchased from Kanto Chem. Co. (Japan). Before use, the PBA sample was first purified by precipitating into ethanol from the chloroform solution. After being isolated by ultracentrifugation, it was dried completely in the vacuum oven at 40 °C for 1 week. PVDF ($M_w$ = 180 000) was purchased from Aldrich Chemical Corp. and used as received.

The PVDF/PBA blends with different compositions were prepared by solution casting using *N*,*N*-dimethylformamide (DMF) as a common solvent. The solutions of PBA and PVDF (the initial concentrations of both polymers are 2 g/100 mL) were mixed with different volume proportions and well stirred. Then, these mixed solutions were cast on the Teflon dishes. After the evaporation of solvent at 80 °C for 1 day, the resultant films were further dried in the vacuum oven at 40 °C for 1 week. Thus, the blends marked as 10/90, 25/75, 50/50, 75/25 and 90/10 were prepared with the first numeral referring to $C_{PVDF}$.

**Measurements.** *Differential Scanning Calorimetry* (*DSC*). The thermal behavior of PVDF/PBA blend was measured by a Pyris Diamond DSC instrument (Perkin-Elmer Japan Co., Tokyo, Japan) equipped with a Perkin-Elmer intracooler 2P cooling accessory. The temperature and heat flow were calibrated using an indium standard with nitrogen purging. For the nonisothermal crystallization, PBA, PVDF, and their blends were melted at 200 °C for 2 min to eliminate the thermal history. Then, they were cooled at a rate of 10 °C/min to −50 °C, followed by reheating to 200 °C at a heating rate of 10 °C/min. For the isothermal crystallization, the samples were rapidly quenched from 200 °C to the desired crystallization temperature of PBA ($T_{c,PBA}$) at a cooling rate of 100 °C/min, followed by reheating to 200 °C at a heating rate of 10 °C/min.

To determine the glass transition temperature ($T_g$), PVDF/PBA blends was analyzed by a DSC 220 system (Seiko Instrument, Tokyo, Japan). After the samples were held at 200 °C for 2 min, they were quenched to −120 °C using liquid nitrogen, followed by reheating to 200 °C at a rate of 10 °C/min, and the DSC curves were recorded. The $T_g$ value was determined as the temperature of the middle point of the transition.

*Wide-Angle X-ray Diffraction* (*WAXD*). In order to prepare the film samples for the WAXD measurement, the samples sandwiched between two iron plates with the thickness of 1 mm were pressed for 2 min at 200 °C under 5 MPa on the hot press (TOYOSEIKI Co., Tokyo, Japan). For the isothermal crystallization, the pressed sample films were quickly thrown into the water bath preset to the $T_{c,PBA}$. For the PBA annealing experiment at 48 °C, the pressed sample films were first thrown into the water bath preset to 18 °C to obtain the pure PBA $\beta$-form and then were transferred into the vacuum oven with 48 °C for various times (10, 30, and 60 min). After the completion of the isothermal crystallization or annealing, the sample films were used for the WAXD measurement. The WAXD patterns were recorded on a Rigaku RU-200 with Ni-filtered Cu K$\alpha$ radiation ($\lambda$ = 0.1542 nm), worked at 40 kV and 200 mA (Rigaku Corp., Tokyo, Japan). The WAXD patterns were collected between Bragg angles of 5°−50° at a scanning rate of 1° min$^{-1}$.

*Fourier Transform Infrared* (*FTIR*) *Spectroscopy*. The transmission FTIR measurements were carried out on the AIM-8800 automatic infrared microscope (Shimadzu, Kyoto, Japan). The samples for FTIR measurements were prepared as follows: the samples sandwiched between two pieces of $BaF_2$ slides were first heated to 200 °C on the hotstage (FP82HT, Mettler-Toledo International Inc., Switzerland), held at this temperature for 2 min to remove the thermal history, and then quickly transferred on the other hotstage (Linkam-600, Japan High Tech Co., Ltd. Fukuoka, Japan) preset to the desired $T_c$. In order to avoid the temperature variation and the thermal lag as far as possible, the hot stage is connected with a set of cooling equipment with liquid nitrogen. To avoid the effect of the temperature on FTIR spectra, these IR spectra were scanned and collected at 20 °C. All the FTIR spectra were collected at an accumulation of 32 scans and a resolution of 2 cm$^{-1}$.

*Polarized Optical Microscopy* (*POM*). POM observation was performed on a BX90 microscopy (Olympus Co., Tokyo, Japan)

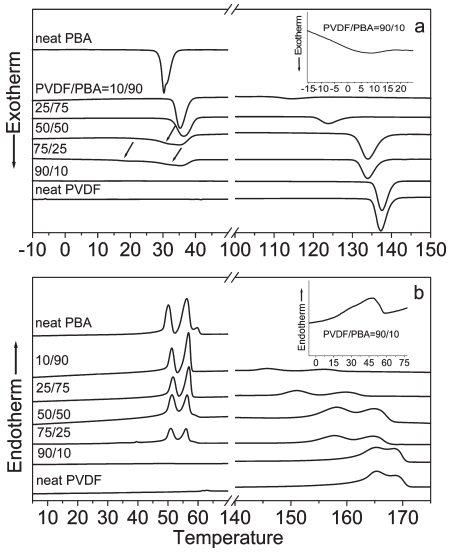


**Figure 1.** DSC cruves of (a) nonisothermal crystallization and (b) subsequent heating for PBA, PVDF, and their blends with various compositions. The thermograms were normalized by the content of PBA component with exception of those of neat PVDF. The insets in panels a and b show the enlarged curves of PBA component with $C_{PVDF} = 90\%$.

equipped with a digital camera. The blend samples were sandwiched between two glass slides and melted at 200 °C for 2 min in a hot stage (Linkam-600). During melting, the samples were pressed slightly to form a thin film with a thickness of ≈0.1 mm. Then, they were quickly transferred to the other hot stage (FP82HT) preset to 145 °C and kept at this temperature for a desired time to crystallize the PVDF component, followed by being quenched to 45 °C to crystallize the PBA component. The photographs were recorded after the complete of crystallization.

## Results and Discussion

**Nonisothermal Crystallization Analysis by DSC.** Figure 1 shows the DSC nonisothermal crystallization curves and the subsequent heating curves of PBA, PVDF, and their blends with different $C_{PVDF}$s. The crystallization (Figure 1a) and melting peaks (Figure 1b) in the low-temperature region are related to the PBA component and those in the high-temperature region to the PVDF component. The $T_{c,PVDF}$ and $T_{m,PVDF}$ are markedly higher than those of PBA. During the cooling process, the crystallization of PVDF component has finished before reaching $T_{c,PBA}$. It can be clearly observed that the crystallization and melting temperatures of the PBA and PVDF component are strongly dependent on the blend composition. In addition, only a single and composition-dependent $T_g$ is discerned for the blends (Table 1), confirming that PVDF is miscible with PBA.

In Table 1 are listed the crystallization temperature ($T_c$) and enthalpy ($\Delta H_c$) during the nonisothermal crystallization, the melting enthalpy ($\Delta H_m$), and the relative crystallinity ($X_c'$) for the PBA and PVDF components in the blends. The crystallization and melting enthalpies of PBA and PVDF have been normalized from their weight percents. As shown in Table 1, except for the blend with $C_{PVDF} = 90\%$, the $T_c$ vlaues of PBA component in the blends are higher than that of the neat PBA, indicating that the addition of PVDF accelarates the crystallization of PBA.

When $C_{PVDF} = 50$ and 75%, the predominant crystallization peak with a shoulder peak (denoted as arrow in Figure 1a) becomes much broader, indicating that the larger amount of PVDF hinders the crystallization of PBA. Interestingly, for the blend with $C_{PVDF} = 75\%$, a weak crystallization peak is discerned at ~18 °C (denoted as arrow in Figure 1a) apart from the predominant crystallization peak at ~35 °C. This suggests that the large amount of PVDF results in the fractional crystallization of PBA component. Moreover, for the blend with $C_{PVDF} = 90\%$, the PBA component shows a wide crystallization peak at about 6 °C (shown in the inset of Figure 1a), suggesting that the excess amount of PVDF dramatically impedes the crystallization of PBA component. On the other hand, with increasing the $C_{PVDF}$, $\Delta H_c$ and $\Delta H_m$ of the PBA component decrease compared to those of the neat PBA, indicative of the decrease in the relative crystallinity ($X_c'$) of the PBA component.

On the basis of the SAXS analyses,[26,27] it has been found that with an increase of $C_{PVDF}$ in the PVDF/PBA blends the PBA component is gradually entrapped into the interlamellar/interfibrillar region from the interspherulitic region of the PVDF matrix. Therefore, the fractional crystallization and well-separated crystallization peaks of the PBA component in the blends with the different $C_{PVDF}$s are probably attributed to the PBA dispersed in the interlamellar/interfibrillar and interspherulitic region of the PVDF matrix.

With increasing the $C_{PBA}$, the $T_c$ value of the PVDF component decreases monotoncially and the crystallization peak becomes wider, as shown in Figure 1 and Table 1. Similarly, $\Delta H_c$, $\Delta H_m$, and $X_c'$ of the PVDF component also decrease with $C_{PBA}$. These results also indicate miscibility between PVDF and PBA.

It is noteworthy that in the PVDF/PBA blend system the $T_g$ of the blend alters relatively slightly from −43.8 °C of the neat PVDF to −60.2 °C of the neat PBA, as shown in Table 1. Althoug the PVDF component shows much higher $T_c$ and $T_m$ than those of the PBA component, its $T_g$ is quite close to that of the PBA component and is significantly lower than $T_c$ of the PBA component. So the effect of $T_g$ on the crystallization behavior and phase separation of the PVDF/PBA blend system can be neglected.

**Crystalline Structure of PBA Component Analyzed by WAXD.** Figure 2 shows the WAXD patterns of the PVDF/PBA blends melt-crystallized at various $T_{c,PBA}$s. As described in the Introduction, only the PVDF α-form can be produced by melt-crystallization at the temperature below 160 °C. Since the diffraction peaks of the PVDF α-form (shown in Figure 2f) in the WAXD pattern are well-separated from those of the PBA component, we can investigate the structural change of the PBA component during the melt-crystallization at various $T_{c,PBA}$s from these diffraction patterns. For clarity, only the WAXD peaks of PBA component are shown in Figure 2a−e.

As seen in Figure 2a, the PBA pure $\beta$-form is developed at $T_c \leq 28$ °C and the pure α-form is formed at $T_c \geq 32$ °C. At $T_c = 29-31$ °C, a mixture of α- and $\beta$-form is developed. After the addition of small amount of PVDF (i.e., $C_{PVDF} = 10\%$ in Figure 2b), the pure α-form is developed at 28 °C, which is lower than the upper critical formation temperature of neat PBA (~32 °C). A distinct peak related to the α(110) peak can be discerned at $T_c = 23$ °C but not at 22 °C, indicating that PBA α-form appears at about $T_c = 23$ °C, which is much lower than the lower critical formation temperature of neat PBA (~29 °C). Therefore, we concluded that the incorporation of small amount of PVDF can greatly lower the $T_c$ of the PBA α-form. The similar results can also be found in other cases with $C_{PVDF} = 25-75\%$, being shown in Figure 2c−e.

At $C_{PVDF} = 90\%$, no diffraction peak assigned to the PBA component can be observed even at $T_c = 0$ °C, and only the (100), (020), (110), and (021) diffraction peaks attributed

**Table 1. Crystallization Temperature ($T_c$), Crystallization and Melting Enthalpy ($\Delta H_c$ and $\Delta H_m$), and Relative Crystallinity ($X_c'$) of the PBA and PVDF Component in the PVDF/PBA Blend System with Different $C_{PVDF}$s during the Nonisothermal Crystallization and Subsequent Heating Process**

| | | PBA component | | | | PVDF component | | | |
|---|---|---|---|---|---|---|---|---|---|
| sample | $T_g$ (°C) | $T_c$ (°C) | $\Delta H_c$ (J/g) | $\Delta H_m$ (J/g) | $X_c'$ (%) | $T_c$ (°C) | $\Delta H_c$ (J/g) | $\Delta H_m$ (J/g) | $X_c'$ (%) |
| neat PBA | −60.2 | 30.3 | −60.6 | 61.5 | 100 | | | | |
| PVDF/PBA = 10/90 | −58.5 | 34.9 | −56.5 | 57.4 | 93 | 113.2 | −33.3 | 28.7 | 65 |
| PVDF/PBA = 25/75 | −56.1 | 36.4 | −52.3 | 51.9 | 84 | 124.1 | −36.1 | 31.4 | 71 |
| PVDF/PBA = 50/50 | −51.4 | 35.1 | −46.5 | 43.7 | 71 | 133.9 | −40.9 | 34.2 | 77 |
| PVDF/PBA = 75/25 | −47.3 | 35.4, 18.3 | −29.2 | 25.3 | 41 | 134.4 | −44.8 | 37.5 | 85 |
| PVDF/PBA = 90/10 | −45.2 | 6.3 | −4.4 | 4.8 | 8 | 138.3 | −48.2 | 42.3 | 96 |
| neat PVDF | −43.8 | | | | | 137.9 | −51.3 | 44.1 | 100 |

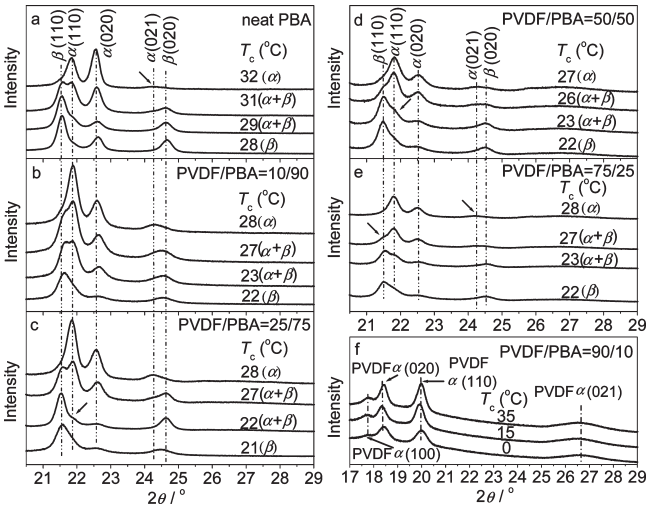


**Figure 2.** WAXD patterns of the PVDF/PBA blend pair melt-crystallized at various temperatures from the homogeneous melt with the content of PVDF of (a) 0, (b) 10, (c) 25, (d) 50, (e) 75 and (f) 90 wt %, respectively. The diffraction peaks associated with the PBA $\beta$- and α-form and PVDF are marked.

to the PVDF α-form can be found,[26] as shown in Figure 2f, suggesting that it is very difficult for the PBA component to crystallize completely; that is, the crystallinity of the PBA component is very low in this case, being in agreement with the aformentioned DSC results during the nonisothermal crystallization process. According to the previous SAXS result,[26,27] when $C_{PVDF}$ = 90%, the PBA component is dispersed in the interlamellar/interfibrillar region of the PVDF matrix which is unfavorable for the crystallizaiton of the PBA component, presenting the solidified matrix and confined space to restrict the chain rearrangement during the crystallization process.

To illustrate the effects of PVDF on the transition temperature of the PBA α- and $\beta$-form, the $T_c$ values of the PBA α- and $\beta$-form are plotted as a function of the $C_{PVDF}$ in Figure 3. In addition, to follow the $T_c$-dependent crystalline structural change of the PBA component, the ratios of the PBA α-form to the PBA crystalline phase (expressed as α%) in the WAXD pattern at various $T_c$s have been quantitively estimated by fitting curve according to the Gauss method.[29] The WAXD pattern of the neat PBA melt-crystallized at 29 °C is chosen as an example and the analytical procedure is shown in Figure 4. Here, α% is defined as the area ratio of the diffraction peaks related to the PBA α-form to that of the whole PBA crystalline phase. The results are shown in Figure 5. From Figures 3 and 5, it can be clearly found that, upon incorporation of PVDF, the critical $T_c$ of the PBA α-form decreases. Moreover, the temperature range of the phase transtion from the $\beta$- to α-form becomes wider.

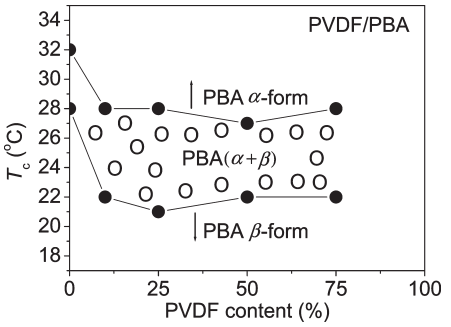


**Figure 3.** $C_{PVDF}$-dependent $T_c$ of the PBA α- and $\beta$-form in the PVDF/PBA blend.

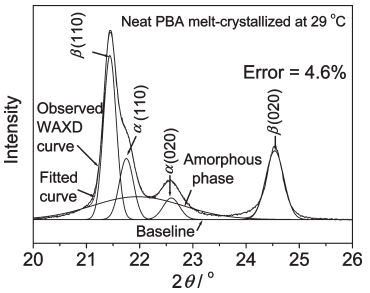


**Figure 4.** Observed and fitted WAXD patterns for the neat PBA melt-crystallized at 29 °C.

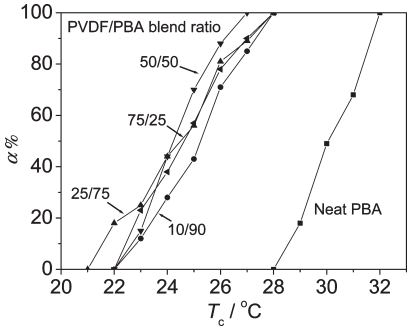


**Figure 5.** $T_c$-dependent α% of the PBA component in the PVDF/PBA blend with different $C_{PVDF}$s.

**Crystalline Structure of PBA Component Analyzed by FTIR.** In our previous study, we have found that the 930 $cm^{-1}$ band is assigned to the characteristic band of the PBA $\beta$-form, and no corresponding characteristic band can be found for the PBA α-form.[5] PVDF shows no absorption peak at around 930 $cm^{-1}$ in its FTIR spectrum, enabling us to differentiate clearly PBA from the PVDF component in the FTIR spectrum of their blend. Figure 6 shows the FTIR spectra and their corresponding second derivatives in

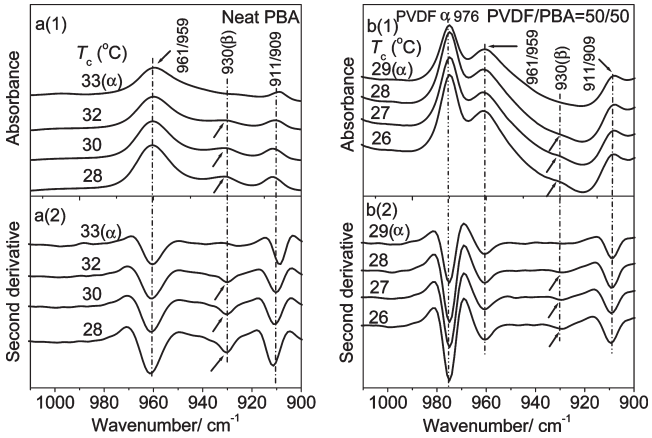


**Figure 6.** FTIR spectra and their corresponding second derivatives in the region of 1010−900 $cm^{-1}$ for the neat PBA and PVDF/PBA blend with $C_{PVDF}$ = 50% melt-crystallized at various temperatures from 200 °C.

the region of 1010−900 $cm^{-1}$ for the neat PBA and the PVDF/PBA blend with $C_{PVDF}$ = 50% melt-crystallized at different $T_c$s.

As seen in Figure 6a(1), apart from two band shifts (from 961 to 959 and 911 to 909 $cm^{-1}$ bands), the neat PBA samples melt-crystallized at ≤32 °C show a peak at 930 $cm^{-1}$, characteristic of the β-form (denoted as arrow), reflecting that the PBA β-form can be found at $T_c \leq 32$ °C. That is, the pure α-form appears at $T_c \geq 33$ °C for the neat PBA. This can be more clearly observed from the second derivatives shown in Figure 6a(2). As shown in Figure 6b, at $C_{PVDF}$ = 50%, two features in the FTIR spectra should be addressed. First, a new peak at 976 $cm^{-1}$ assigned to the PVDF α-form[30] appears. Second, the 930 $cm^{-1}$ band can be discerned at $T_c \leq 28$ °C; that is, the pure α-form of the PBA component appears at $T_c \geq 29$ °C, which is lower than 33 °C for the neat PBA. The similar results can be found in other compositions with exception of $C_{PVDF}$ = 90% where no absorption peak related to the PBA component can be discerned.

**Isothermal Crystallization Analyzed by DSC.** The isothemral crystallization and the subsequent melting behavior of the PBA component have also been investigated in detail. The Avrami kinetic parameters (the Avrami exponent $n$, the crystallization half-time $t_{1/2}$, and the crystallization rate constant $k$) of the neat PBA and the PBA component in this blend system melt-crystallized at various $T_c$s were analyzed by using the Avrami equation[31−33] (the DSC isothermal crystallization curves are not shown). Here, the DSC crystallization behavior observed at three $T_c$s—25, 30, and 35 °C—are selected as examples, and their Avrami kinetic parameters are summarized in Table 2. The Avrami exponent ($n$) is strongly influenced by the mode of nucleation, that is, homogeneous or heterogeneous nucleation, and the dimension of the crystal growth. It is a combined function of the time dependence of nucleation ($n_1$) and the number of dimension ($n_2$) in which crystal growth occurs and can be expressed as $n = n_1 + n_2$.[32] Nucleation is either instantaneous, e.g., heterogeneous nucleation with $n_1 \approx 0$ with nuclei appearing all at once in the early stage of crystallization, or sporadic, e.g., homogeneous nucleation with $n_1 \approx 1$ with the number of nuclei increases with time.[32] $n_2$ = 1, 2, and 3 represent respectively one-, two-, and three-dimensional growth. In practice, the obtained $n$ value by the Avrami equation is not an integer for some uncertain factors.

For the neat PBA sample, the experimentally estimated $n$ values are all close to 4 regardless of the $T_c$ value, indicating that the neat PBA spherulites grow with a three-dimensional manner in a homogeneous growth mode. When $C_{PVDF}$ = 10 and 25%, the $n$ values are close to 3, suggesting that the PBA crystals still grow with a three-dimensional manner but in a heterogeneous growth mode. With $C_{PVDF}$ = 50 and 75%, the $n$ values are close to 2, revealing that the PBA crystals develop mainly with a planar two-dimension manner in the solidified PVDF matrix; that is, the PBA crystal in a relatively narrow space, as in this case, could not grow freely in a three-dimensional manner. In addition, the $t_{1/2}$ values decrease and the $k$ values increase for the PBA component with $C_{PVDF}$ = 10 and 25% compared to those of the neat PBA at the same $T_c$, indicating that the small amount of PVDF increases the crystallization rate of PBA component. It is notable that when $C_{PVDF}$ = 50%, the $t_{1/2}$ and $k$ values of the PBA component are nearly the same to those of the neat PBA at the same $T_c$; when $C_{PVDF}$ = 75%, the crystallization rate of the PBA component decreases rather than increases, suggesting that the large amount of PVDF would greatly hinder the crystallization of the PBA component. If the excess amount of PVDF ($C_{PVDF}$ = 90%) is incorporated, the PBA component cannot crystallize at all.

With combination of the aforementioned nonisothermal crystallization data and the previously reported SAXS results,[26,27] the dual effect of PVDF on the crystallization behavior of the PBA component can be proposed. That is, first, the small amount of PVDF in the solid state serves as the nucleating agent to accelerate the crystallization of the PBA component for presenting the foreign surface to PBA where the heterogeneous nucleation occurs, which results in the enhancement of nucleation rate of the PBA component. Second, the large amount of PVDF acts as the solidified matrix to provide many confined and restricted spaces to hinder the crystallization of the PBA component, which is unfavorable for the PBA component to adjust its chain packing during the crystallization process.

Figure 7 shows the melting curves of the neat PBA and the PBA component after melt-crystallization at different $T_{c,PBA}$s. From Figure 7a, it can be seen that the β-form of the neat PBA melt-crystallized at $T_c$ = 29 °C shows two melting peaks denoted as $T_{m1}$ and $T_{m2}$. In the temperature region of 30−32 °C, a mixture of the PBA α- and β-form develops, and it shows three melting peaks denoted as $T_{m5}$, $T_{m6}$, and $T_{m7}$ with the intensity of the melting peak $T_{m7}$ gradually decreasing. With a further increase in $T_c$ (i.e., 33 °C), the pure α-form develops with two melting peaks denoted as $T_{m3}$ and $T_{m4}$. It can be found that from Figure 7a these two melting peaks ($T_{m1}$ and $T_{m2}$) of the PBA β-form are slightly higher than the corresponding two peaks ($T_{m3}$ and $T_{m4}$) of the α-form. The DSC result is also similar to the previous reports.[8,9] Upon addition of small amount PVDF (for example, $C_{PVDF}$ = 10 and 25% as shown in Figure 7b,c), the formation temperature of the pure α-form (33 and 32 °C) changes little as compared to that of the neat PBA (33 °C). However, the temperatures at which the PBA α-form appears in the above two cases (< 22 °C) are greatly lower than that for the neat PBA (30 °C). With further increasing the $C_{PVDF}$ to 50 and 75%, the $T_c$ for the pure α-form (30 °C) decreases by 3 °C compared to that for the neat PBA. It can be also concluded that PVDF is favorable for the formation of the PBA α-form. With $C_{PVDF}$ = 90%, as shown in Figure 7f, almost no PBA melting peak can be observed even at $T_c$ = 0 °C, reflecting again that the crystallizability of the PBA component significantly decreases in this blend.

It needs to be mentioned that the DSC results mentioned in Figure 7 are not always the same to the WAXD results

**Table 2. Avrami Kinetics Parameters of the Isothermal Crystallization for the PBA Component in the PVDF/PBA Blend with Different $C_{PVDF}$s**

| | isothemal crystallization of PBA | | | | | | | | | |
|---|---|---|---|---|---|---|---|---|---|---|
| | 25 °C | | | 30 °C | | | 35 °C | | | |
| sample | $n$ | $t_{1/2}$ (min) | $k$ (min$^{-1}$) | $n$ | $t_{1/2}$ (min) | $k$ (min$^{-1}$) | $n$ | $t_{1/2}$ (min) | $k$ (min$^{-1}$) | $T_m^0$ of the PBA α-form crystal (°C) |
| neat PBA | 3.7 | 0.35 | 9.3 | 4.1 | 0.49 | 6.4 | 3.9 | 1.7 | 0.94 | 61.3 |
| PVDF/PBA = 10/90 | 2.8 | 0.21 | 19.1 | 3.2 | 0.28 | 11.5 | 2.9 | 1.1 | 1.35 | 57.9 |
| PVDF/PBA = 25/75 | 2.6 | 0.25 | 12.7 | 2.8 | 0.31 | 9.1 | 2.8 | 0.9 | 1.87 | 54.4 |
| PVDF/PBA = 50/50 | 2.2 | 0.33 | 9.7 | 2.2 | 0.46 | 6.9 | 2.4 | 1.6 | 1.01 | 55.8 |
| PVDF/PBA = 75/25 | 1.9 | 0.38 | 8.4 | 2.1 | 0.53 | 5.3 | 2.1 | 2.1 | 0.81 | 56.2 |
| PVDF/PBA = 90/10 | —[a] | —[a] | —[a] | —[a] | —[a] | —[a] | —[a] | —[a] | —[a] | —[a] |

[a] Unable to be estimated.

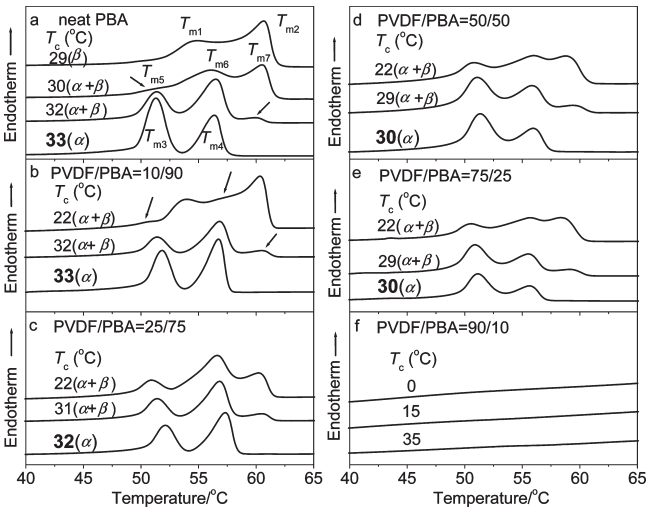


**Figure 7.** DSC heating curves of the neat PBA and the PBA component in the PVDF/PBA blend quenched from 200 °C and melt-crystallized at various $T_c$s.

shown in Figure 2, especially for the formation temperature of the pure α-form. It is probably attributed to the difference of the cooling rate between the WAXD and DSC measurement. For the WAXD measurement, the sample is directly thrown into the water bath preset to the desired $T_{c,PBA}$s. However, for the DSC measurement, it needs a short time to get to the $T_{c,PBA}$s even at a high cooling rate of 100 °C/min. Furthermore, there is a possibility that the crystallization of the PBA β-form has finished before reaching the predetermined $T_{c,PBA}$s due to its own significantly great crystallization rate which is probably further increased by the PVDF component. This point could be confirmed from the DSC isothermal crystallization curves (data not shown). Therefore, upon the incorporation of PVDF, it seems that no pure PBA β-form develops during the cooling process in the DSC measurement. All of the WAXD, FTIR, and DSC results indicate that the crystalline structure of the PBA component is affected by the miscible blending with PVDF, and an addition of PVDF is favorable for the formation of the PBA α-form.

From the viewpoint of thermodynamics, the equilibrium melting point ($T_m^0$) of the neat PBA and the PBA component in this blend is expected to provide the evidence of the depression of $T_c$ for the PBA α-form. A simple and extensively accepted method, that is, the Hoffman−Weeks method,[34] was utilized to draw a plot of $T_c$ vs $T_m$ to estimate the $T_m^0$ of the PBA α-form. As the pure PBA β-form cannot be obtained in the PVDF/PBA blend system in the DSC measurement with the cooling rate of 100 °C/min, the $T_m^0$ value was not estimated for the β-form. Here, the first melting temperature of the pure PBA α-form is chosen for the determination of $T_m^0$. The experimental data can be extrapolated to the intersection with a line of $T_c = T_m$ and the temperature at the intersection is the $T_m^0$. The $T_m^0$ values are listed in Table 2. It can be found that after blending with PVDF all the $T_m^0$ values of the PBA α-form with exception of $C_{PVDF}$ = 90% (57.9, 54.4, 55.8, and 56.2 °C) are lower than that of the neat PBA (61.3 °C). That is, an addition of PVDF results in the depression of $T_m^0$ of the PBA α-form, which is also an indicative of miscibility between PVDF and PBA. Accordingly, the depression of $T_m^0$ upon blending would shift correspondingly the crystallization temperature window to the low-temperature region and thus decreases the critical $T_c$.[35]

However, the change in the $T_m^0$ value of the PBA α-form upon incorporation of PVDF is relatively samll with lowering of 3.4−6.8 °C. Therefore, it is probably concluded that, in addition to the thermodynamic effect, the kinetics maybe an important contribution for the crystalline structure upon blending. According to the classical metastable theory,[35,36] the metastable phases are considered to fall into one of the multiple local free energy minima in the Gibbs free energy profiles and will ultimately transform into the thermodynamically stable state of global free energy minimum. Among the crystal forms, all but one are metastable state at a specific temperature and pressure. As a metastable phase, the fomation of the PBA β-crystal is usually due to the kinetic effects which provide a favorable pathway for the polymer to fall into the local free energy minimum.[9,35,36] Because of the kinetically preferential growth of the PBA β-form and the reduction of the surface free energy of nucleus upon blending with PVDF, it is favorable for the formation of the PBA α-form at the lower $T_c$.

**Phase Transition of PBA upon Annealing.** To investigate the effect of PVDF on the PBA phase transition, the neat PBA and PVDF/PBA blend system were annealed at 48 °C for various periods after melt-crystallization at 18 °C to produce the pure β-form. As shown in Figure 8a, after annealing at 48 °C for 10 min, almost no diffraction peak related to the α-form can be discerned for the neat PBA. When the annealing time is increased to 30 or 60 min, only a very weak shoulder peak associated with the α (110) peak can be observed, indicating that after annealing at 48 °C for 1 h only a small amount of the PBA β-form can be transformed into the α-form. However, upon incorporation of small amounts of PVDF, i.e., 10%, the β-form is dramatically quickly and completely transformed into the pure α-form in the time length of less than 10 min, as presented in Figure 8b, suggesting that PVDF could significantly accelerate the PBA phase transition from the β- to the α-form.

When $C_{PVDF}$ = 25%, as shown in Figure 8c, most of the β-form has been transformed into the α-form after annealing for 10 min, and only a very weak peak related to the β (110) diffraction (denoted by arrow) can be detected.

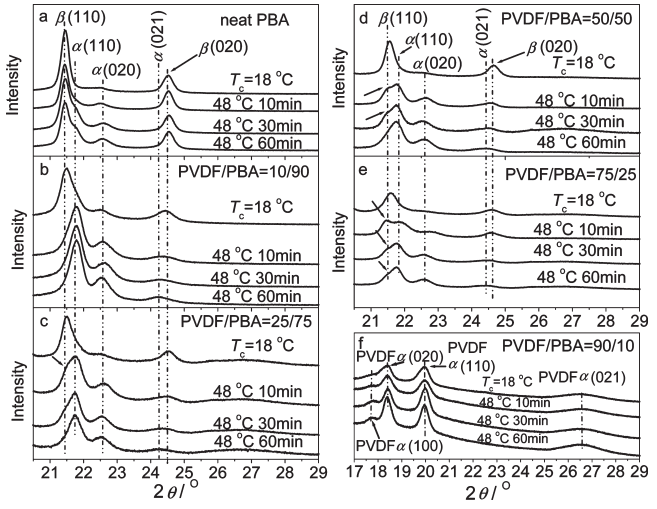


**Figure 8.** WAXD patterns of the PVDF/PBA blend first melt-crystallized at 18 °C and then annealed at 48 °C for various periods.

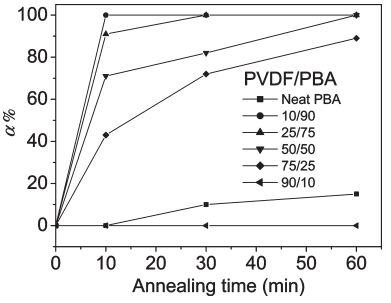


**Figure 9.** Annealing time-dependent α% of the PBA component in the PVDF/PBA blend with different $C_{PVDF}$s.

The predominant peak is attributed to the α (110). If the annealing time is raised to 30 min, the $\beta$-form can be completely transformed into the α-form. With further increasing $C_{PVDF}$ to 50%, as shown in Figure 8d, a small amount of the PBA $\beta$-form still resides after annealing for 30 min; that is, the whole phase transition needs longer time annealing in this case. When $C_{PVDF}$ = 75%, it costs more than 60 min annealing to finish the whole phase transition, though most of the $\beta$-form has been transformed into the α-form with 60 min annealing. Anyway, the rate of phase transition of the PBA $\beta$-form in the blend system is still greatly larger than that of the neat PBA. If $C_{PVDF}$ = 90%, no diffraction peak related to the PBA component is detectable even annealing at 48 °C for 60 min.

To quantitatively evaluate the phase transition process, the ratio of the PBA α-form to the PBA crystalline phase (α%) of the neat PBA and the PBA component in this blend system annealed at 48 °C for various times have been calculated according to the analytical procedure, as shown in Figure 4. The results are presented in Figure 9. From Figure 9, it can be clearly observed that, with exception of the case with $C_{PVDF}$ = 90%, the addition of PVDF highly speeds up the rate of the PBA phase transition from the $\beta$- to α-form. After annealing at 48 °C for 60 min, the amount of the transformed α-form for the neat PBA is less than 20%, which is significantly lower than those in other four cases with $C_{PVDF}$ = 10, 25, 50, and 75%. On the other hand, the large amount of PVDF would decelerate the phase transition of PBA to a certain extent. Upon annealing for 10 min, the PBA $\beta$-form has been completely transformed into the α-form in the blend with $C_{PVDF}$ = 10%, while the amounts of the transformed α-form are 91, 71 and 42% for the three blends with $C_{PVDF}$ = 25, 50, and 75%, respectively.

On the basis of the above WAXD results, the effect of PVDF on the phase transition of PBA can be summarized as two points. First, PVDF is favorable to the phase transition of PBA from the $\beta$- to α-form during the annealing process and significantly shortens the period of phase transition, compared to that of the neat PBA. On the other hand, the small amount of PVDF greatly accelerates the phase transition while the large amounts of PVDF would decelerate the phase transition. The reasons are probably attributed to three points. First, the enough energy is needed to overcome the energy barrier for the phase transition.[9] It has been reported[9] that the annealing at 40 °C for 1 h only results in the thickening of the lamellar and could not realize the phase transition of the PBA $\beta$-form for not enough energy available for the phase transtion; that is, the accumulated energy after annealing at 40 °C for 1 h is still lower than the critical energy barrier used for the phase transition. Upon addition of PVDF, the critical $T_c$ of the PBA α-form decreases, suggesting that the critical energy barrier for the phase transition decreases, too. Accordingly, at the same annealing temperature (in this case, $T_a$ = 48 °C), because of the greater temperature difference of ($T_a - T_{c,a}$) in the presence of PVDF, it can provide more energy to speed up the phase transition of the PBA. Therefore, the obtained energy during the annealing is the predominant driving force to realize the phase transition. Second, because of the physically confined effect of the solidified PVDF matrix in the PVDF-rich case, it is unfavorable for the adjustment of the PBA molecular chain during the phase transition for the different packing manner between the PBA $\beta$- and α-form. Third, the large amount of PVDF, acting as a diluent, probably hinders the structural adjustment of the PBA component and decreases the transition rate to a certain extent.

**Morphology Observation by POM.** To observe the phase distribution of PVDF and PBA in these blends, their morphologies were investigated by POM. Here, the POM micrographs of the PVDF/PBA blends with $C_{PVDF}$ = 10, 50, and 90% are chosen as representatives. The blend samples were first quickly cooled from 200 to 145 °C and kept at this temperature for 24 h to completely crystallize the PVDF component, then quenched to 45 °C, and kept at this temperature for 3 h to crystallize the PBA component.

From Figure 10a, it can be found that because of the diluting effect of the PBA component at 145 °C, the very small amount of PVDF is distributed (denoted as arrow) in the molten PBA. With being quenched to 45 °C to crystallize completely the PBA component, as shown in the Figure 10b, apart from the small amount PVDF spherulite, the brightness which is attributed to the refringence of the large amount of the PBA spherulite becomes greatly stronger, suggesting that the predominant region is occupied by the PBA spherulites and PVDF is only sporadically dispersed among the PBA spherulites. It is documented that the PVDF α-crystal shows the monoclinic unit cell with dimensions of $a$ = 0.496 nm, $b$ = 0.964 nm, $c$ = 0.468 nm;[37] the PBA α-crystal is packed in a monoclinic cell with dimensions of $a$ = 0.673 nm, $b$ = 0.794 nm, $c$ = 1.416 nm, and the $\beta$-crystal possesses the orthorhombic unit cell with dimensions of $a$ = 0.506 nm, $b$ = 0.735 nm, $c$ = 1.467 nm.[6] The length of the $c$ axis of the PBA α-crystal is about thrice that of the $c$ axis of the PVDF α-crystal, and the length of $a$ axis of the PBA $\beta$-crystal is relatively close to that of $a$ axis of the PVDF α-crystal. The relatively good lattice matching between the PVDF α-crystal and PBA suggests that the PBA crystals probably grow on the surface of the PVDF crystal which acts

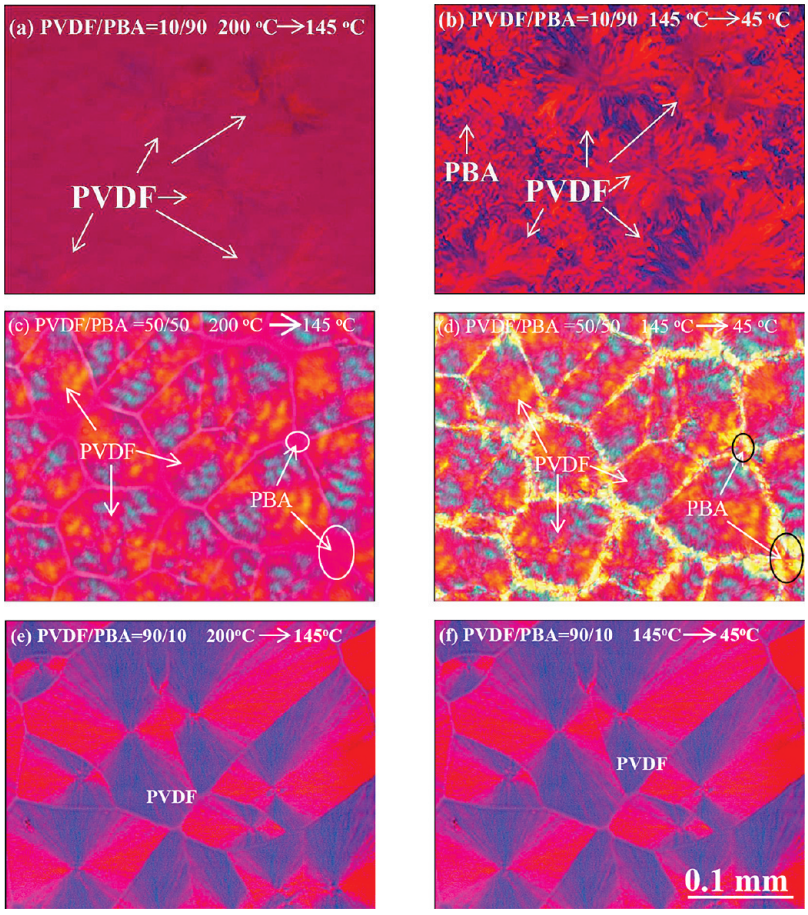


**Figure 10.** POM micrographs of the PVDF/PBA blend with $C_{PVDF}$ = 10% (a, b), 50% (c, d), and 90% (e, f). The blend samples were first cooled to 145 °C and kept at this temperature for 24 h to completely crystallize the PVDF component from 200 °C and then quenched to 45 °C to crystallize the PBA component.

as the nucleating agent by an epitaxial mechanism. Similar phenomena have been reported for zinc phenylphosphonate (PPZn)/poly(L-lactide) (PLLA) composite[38] and the uracil/poly[(3-hydroxybutyrate)-*co*-(3-hydroxyhexanoate)] (PHBHHx) system.[32] In addition, it can be observed that the size is much lower and the density is much larger for the PBA spherulite upon incorporation of a small amount of PVDF than those of the neat PBA at 45 °C (data not shown), probably revealing that a small amount of PVDF as a nucleating agent speeds up the crystallization of PBA.

With increasing the amount of PVDF, i.e., $C_{PVDF}$ = 50%, the very narrow gaps (namely, the molten PBA) among the spherulites of PVDF can be observed, as shown in Figure 10c, indicating the PVDF fills in the predominant region in this case. With decreasing the temperature to 45 °C, it can be more clearly seen that PBA is restricted among the PVDF spherulites, as denoted in the ellipse in Figure 10d. The limited space probably impedes the motion of the molecular chains during the phase transition for the PBA component.

Further increasing the content of PVDF to 90%, PVDF melt-crystallized at 145 °C forms the compact and directly impinged spherulite with a closed structure and occupies completely the whole region, as shown in Figure 10e. Even if the temperature is decreased to 45 °C (Figure 10f), no enhanced brightness related to the PBA spherulite can be found. In this case, PBA is completely entrapped into the interlamellar/interfibrillar region of the PVDF matrix. By the POM and atomic force microscopy (AFM) measurements, the PBA component has also been found to be dispersed in the interspherulitic, interlamellar, and interfibrillar region of the PBS matrix in the PBS/PBA blend depending on the content ($C_{PBS}$) and the crystallization temperature ($T_{c,PBS}$) of the PBS component.[39]

## Conclusion

A small amount of PVDF increases the crystallization rate of PBA, but a large amount of PVDF decreases the crystallization rate of PBA. These dual effects of PVDF on the crystallization behavior of the PBA component can be concluded. First, a small amount of PVDF in the solid state serves as the nucleating agent for PBA component. Second, the large amount of PVDF acts as the solidified matrix to provide many confined and restricted spaces to hinder the crystallization of the PBA component.

From the WAXD and FTIR analyses, it was found that PVDF decreases the $T_c$ of the PBA α-form; namely, the PBA polymorphism can be regulated by PVDF. This can be related to the thermodynamic and kinetic effects. From the WAXD analysis of the phase transition during the annealing treatment, it was found that PVDF significantly accelerates the phase transition of the PBA component from the $\beta$- to α-form, as compared to the neat PBA, whereas a large amount of PVDF would decelerate the phase transition. This is mainly ascribed to three points: (1) the decrease of critical energy barrier (or the supply of more enengy), (2) the physically confined effect of the large amount of the solidified PVDF, and (3) the diluting effect of the large amount of PVDF. In conclusion, PBA polymorphic crystalline structure can be controlled by blending with PVDF.

## References and Notes


(1) Ren, J.; Fu, H. Y.; Ren, T. B.; Yuan, W. Z. *Carbohydr. Polym.* **2009**, *77*, 576–582.
(2) Noguchi, K.; Kondo, H.; Ichikawa, Y.; Okuyama, K.; Washiyama, J. *Polymer* **2005**, *46*, 10823–10830.
(3) Yuan, H.; Liu, Z.; Ren, J. *Polym. Eng. Sci.* **2009**, *49*, 1004–1012.
(4) Lu, J.; Qiu, Z.; Yang, W. *Polymer* **2007**, *48*, 4196–4204.
(5) Yang, J.; Li, Z.; Pan, P.; Zhu, B.; Dong, T.; Inoue, Y. *J. Polym. Sci., Part B: Polym. Phys.* **2009**, *47*, 1997–2007.
(6) Minke, R.; Blackwell, J. *J. Macromol. Sci., Phys.* **1979**, *B16*, 407–417.
(7) Minke, R.; Blackwell, J. *J. Macromol. Sci., Phys.* **1980**, *B18*, 233–255.
(8) Gan, Z.; Abe, H.; Doi, Y. *Macromol. Chem. Phys.* **2002**, *203*, 2369–2374.
(9) Gan, Z.; Kuwabara, K.; Abe, H.; Iwata, T.; Doi, Y. *Biomacromolecules* **2004**, *5*, 371–378.
(10) Woo, E. M.; Wu, P. L.; Wu, M. C.; Yan, K. C. *Macromol. Chem. Phys.* **2006**, *207*, 2232–2243.
(11) Pan, P.; Inoue, Y. *Prog. Polym. Sci.* **2009**, *34*, 605–640.
(12) Gan, Z.; Kuwabara, K.; Abe, H.; Iwata, T.; Doi, Y. *Polym. Degrad. Stab.* **2005**, *87*, 191–199.
(13) Dong, T.; Kai, W.; Inoue, Y. *Macromolecules* **2007**, *40*, 8285–8290.
(14) Kai, W.; Zhu, B.; He, Y.; Inoue, Y. *J. Polym. Sci., Part B: Polym. Phys.* **2005**, *43*, 2340–2351.
(15) Jiang, N.; Zhao, L.; Gan, Z. *Polym. Degrad. Stab.* **2010**, *95*, 1045–1053.
(16) Sun, Y.; Li, H.; Huang, Y.; Chen, E.; Zhao, L.; Gan, Z.; Yan, S. *Macromolecules* **2005**, *38*, 2739–2743.
(17) Sun, Y.; Li, H.; Huang, Y.; Chen, E.; Gan, Z.; Yan, S. *Polymer* **2006**, *47*, 2455–2459.
(18) Wu, M. C.; Woo, E. M. *Polym. Int.* **2005**, *54*, 1681–1688.
(19) Schneider, S.; Drujon, X.; Lotz, B.; Wittmann, J. C. *Polymer* **2001**, *42*, 8787–8798.
(20) Prest, W. M., Jr.; Luca, D. J. *J. Appl. Phys.* **1975**, *46*, 4136–4143.
(21) Lovinger, A. J. *J. Polym. Sci., Polym. Phys. Ed.* **1980**, *18*, 793–809.
(22) Lovinger, A. J.; Keith, H. D. *Macromolecules* **1979**, *12*, 919–924.
(23) Isayeva, I.; Kyu, T.; Manley, R. St. J. *Polymer* **1998**, *39*, 4599–4608.
(24) Penning, J. P.; Manley, R. St. J. *Macromolecules* **1996**, *29*, 77–83.
(25) Penning, J. P.; Manley, R. St. J. *Macromolecules* **1996**, *29*, 84–90.
(26) Liu, L.; Chu, B.; Penning, J. P.; Manley, R. St. J. *Macromolecules* **1997**, *30*, 4398–4404.
(27) Liu, L.; Chu, B.; Penning, J. P.; Manley, R. St. J. *J. Polym. Sci., Part B: Polym. Phys.* **2000**, *38*, 2296–2308.
(28) He, Y.; Zhu, B.; Kai, W.; Inoue, Y. *Macromolecules* **2004**, *37*, 8050–8056.
(29) Dong, T.; He, Y.; Shin, K.; Inoue, Y. *Macromol. Biosci.* **2004**, *4*, 1084–1091.
(30) Buckley, J.; Cebe, P.; Cherdack, D.; Crawford, J.; Ince, B. S.; Jenkins, M.; Pan, J.; Reveley, M.; Washington, N.; Wolchover, N. *Polymer* **2006**, *47*, 2411–2422.
(31) Im, S. S.; Kim, T. J.; Han, S.; Moon, T. J.; Bae, Y. C. *J. Appl. Polym. Sci.* **1997**, *65*, 1745–1750.
(32) Pan, P.; Liang, Z.; Nakamura, N.; Miyagawa, T.; Inoue, Y. *Macromol. Biosci.* **2009**, *9*, 585–595.
(33) Yang, J.; Pan, P.; Dong, T.; Inoue, Y. *Polymer* **2010**, *51*, 807–815.
(34) Hoffman, J. D.; Weeks, J. J. *J. Res. Natl. Bur. Stand.* **1962**, *66A*, 13–28.
(35) Pan, P.; Liang, Z.; Zhu, B.; Dong, T.; Inoue, Y. *Macromolecules* **2009**, *42*, 3374–3380.
(36) Keller, A.; Cheng, S. Z. D. *Polymer* **1998**, *39*, 4461–4487.
(37) Hasegawa, R.; Takahashi, Y.; Chatani, Y. *Polym. J.* **1972**, *3*, 600–610.
(38) Pan, P.; Liang, Z.; Cao, A.; Inoue, Y. *ACS Appl. Mater. Interfaces* **2009**, *1*, 402–411.
(39) Wang, H.; Gan, Z.; Schultz, J. M.; Yan, S. *Polymer* **2008**, *49*, 2342–2353.